PILOT-AIDED ASYMMETRICALLY CLIPPED OPTICAL OFDM IN VISIBLE LIGHT COMMUNICATION

Osama Saied[1], Zabih Ghassemlooy[1], Xuewu Dai[1], Hoa Le Minh[1], Wasu Popoola[2] , Shien-Kuei Liaw[3] , Min. Zhang [4]

[1]Optical Communications Research Group, NCRLab, Faculty of Engineering and Environment, Northumbria University, Newcastle Upon Tyne, NE1 8ST, UK

{osama.saied, z.ghasslooy, hoa.l-minh, xuewu.dai}@northumbria.ac.uk

[2]Institute for Digital Communications, School of Engineering, The University of Edinburgh,

, w.popoola@ed.ac.uk

[3]Department of Electronic Engineering, National Taiwan University of Science and Technology, Taipei 106, Taiwan, skliaw@mail.ntust.edu.tw

[4]The State Key Laboratory of Information Photonics and Optical Communications, Beijing University of Posts & Telecommunications, Beijing,

mzhang@bupt.edu.cn

ABSTRACT

In this paper we present a new pilot-aided asymmetrically clipped optical orthogonal frequency division multiplexing (PA-ACO-OFDM) signaling scheme for intensity modulation direct detection based visible light communications, in the transmission process, amplitude known pilot chips (PCs) are inserted prior to inverting negative chips (NC) into positive chips. At the receiver, PCs are used to detect and recover the NC, thus allowing complete recovery of the OFDM symbols. In this scheme we utilize the anti-asymmetry nature of the time-domain ACO-OFDM signal to increase the data rate by up to 33%. A comparison between PA-ACO-OFDM, DCO-OFDM schemes in terms of the optical power requirements is also presented. We show that the proposed system requires lower optical power compared to DCO-OFDM. Simulation results are presented and it is shown that in the proposed pilot-aided ACO-OFDM data rates are enhanced by reducing the time symbol duration. We also show that the power efficiency and the bit-error-rate performance of the new PA-ACO-OFDM can be enhanced by varying the amplitude of the pilot chips.

KEYWORDS OFDM, visible light communications**.**

1. INTRODUCTION

Visible Light communications (VLCs) using light emitting diodes (LEDs) can provide illuminations, data communications and localization (mostly indoor) in the visible wavelength range of 380 to 780 nm [1], [2]. Compared to the wireless radio frequency (RF) technologies VLCs offer advantages including high energy efficiency, inherent security, no electromagnetic interference and ample unregulated bandwidth [1], [2], [3], [4]. Orthogonal frequency divisions multiplex (OFDM) is a multi-carrier modulation scheme that deals with multipath induced inter symbol interference (ISI) in a highly dispersive channel. OFDM can be combined with any multiplexing schemes as well as the antenna arrays at the transmitter (Tx) and receiver (Rx) to increase the diversity gain and/or enhance the system capacity, and reduce the frequency selective fading [3], [5], [6]. In VLCs the high peak average to power ratio (PAPR), which is one of the major disadvantages of OFDM in RF based systems, has been exploited as an advantage [7]. As such, OFDM has attracted much attention for use in VLCs in recent years [8], [9].

In intensity modulation and direct detection (IM/DD) based VLCs the complex and bipolar signal formats such as the traditional OFDM cannot be used since the light intensity cannot be complex or negative values [1], [10], [11]. To overcome this problem a number of different OFDM formats have been proposed [12], [13], [14], [15]. Among them DC-biased optical OFDM (DCO-OFDM) and asymmetrically clipped optical OFDM (ACO-OFDM) are the two most popular techniques adopted in IM/DD VLCs [15], [16]. Both schemes are constrained to have Hermitian symmetry in order to offer real-time domain signals at the cost of half of the available bandwidth [9], [11], [15], [17].

In DCO-OFDM, a DC bias is added to the signal prior to clipping the negative residual signals in order to ensure all-positive OFDM signal. However, a large DC bias requires a much higher mean optical power. In addition clipping the negative residual signals will result in clipping the noise signal. Meanwhile in ACO-OFDM only the odd subcarriers are demodulated to ensure anti-asymmetric time domain signals, thus clipping the negative signals at a zero level does not lead to loss of information. Consequently, ACO-OFDM is more efficient in term of the optical power requirement compared to on-off-keying (OOK) for example, and has a low clipping noise level, whereas DC-OFDM is more bandwidth efficient [9].

In this paper we present a novel OFDM technique in which the advantages of ACO-OFDM with the anti-asymmetric time domain characteristics are investigated in order to increase the data rate R. This is achievable by employing a reduced number of time slots T_s required to transmit an OFDM symbol. The negative time domain chips are inverted to make them positive, following the insertion of higher amplitude pilot chips (PCs). At the Rx, PCs are used to detect and recover the NC, thus allowing a complete recovery of the OFDM symbols. In this scheme the anti-asymmetry nature of the time-domain ACO-OFDM signal is utilized to increase R by up to almost 33%. The results show that the proposed PA-ACO-OFDM data rates are enhanced by reducing the time symbol duration. We also present that the required optical power of the new system is reduced compared to DCO-OFDM. Furthermore, the power efficiency and the bit error rate (BER) performance of the novel PA-ACO-OFDM can be enhanced by varying the amplitude of the pilot chips.

The rest of the paper is organized as follows. Section 2 gives a description of the proposed PA-ACO-OFDM scheme. In Section 3, the signal analysis of the new system is presented. Results obtained for the proposed scheme is analyzed and evaluated in Section 4. Finally; conclusions are drawn in Section 5.

2. SYSTEM DESCRIPTION

This section gives a brief description of the proposed PA-ACO-OFDM system, including the structures of both Tx and Rx.

2.1. The Transmitter of the new system

Fig. 1 shows a block diagram of the Tx for PA-ACO-OFDM. Although it is similar to the standard ACO-OFDM the main differences are the inclusion of anti-symmetric signals removal, pilot insertion (PI) and the negative inversion blocks. The signal processing procedure is described as below: First, a sequence of serial binary data $bi(t)$ ($bi \in \{1,0\}$) is mapped into a group of complex quadrature amplitude modulation (QAM) symbols S_{QAM} according to the chosen modulation scheme, such as 4-, 16-, 128-…. and 1024-QAM. Similar to the standard ACO-OFDM in which only the odd subcarriers (SC) carry the data symbols to meet the requirement of non-negative time-domain signals, S_{QAM} are allocated to the odd SCs only and all the symbols on the even SCs are set to zero. The resulting signal Z is further processed to maintain Hermitian symmetry (HS) as defined in [11]. As in all OFDM systems, the output of HS X is in the frequency-domain, which is converted back into the time domain using IFFT.

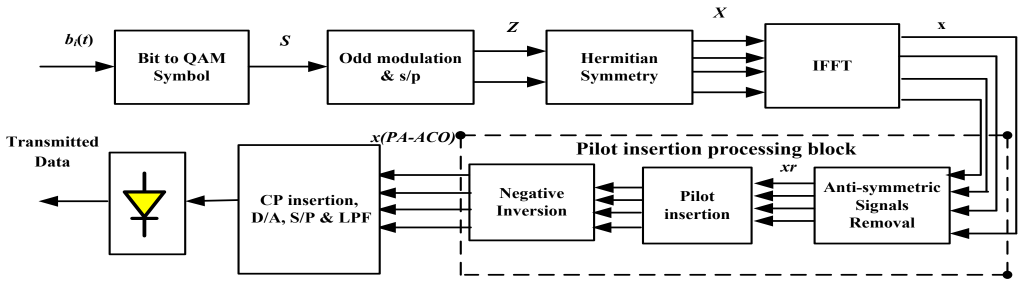

Fig. 1. Block diagram of the pilot-aided ACO-OFDM transmitter

The OFDM symbol in the time domain x indeed is a sequence of chips. The odd modulation and HS process are implemented prior to IFFT to obtain an anti-symmetric and real time domain sequence of chips. However, the anti-symmetry profile will result in redundant chips. This is because half of the chips in the time domain are repeated anti-symmetrically. It can be shown that only half of the available chips are indeed the information chips carrying $bi(t)$, whereas the other half are 'repeated' but in an anti-symmetric format. From the viewpoint of information, half of the available T_s are redundant and 'wasted' in order to maintain the anti-symmetry profile for real non-negative IM. As a result, the efficiency of ACO-OFDM is quite low and its R is only half that of DCO-OFDM. Improving the bandwidth efficiency and throughput is the main motivation of this paper. To achieve this, the PA-ACO-OFDM scheme is proposed by inclusion a new pilot insertion processing (PIP) block between IFFT and optical modulation blocks, see Fig. 1.

The PIP block consists of three modules. (i) Anti-symmetric signal removal- where the second part of x is removed with the resulting signal x_r having a shorter duration than the standard ACO-OFDM. Removing the second part of x does not lead to loss of information due to the anti-symmetry and redundancy associated with the ACO-OFDM symbol. In doing so, R can be increased since OFDM symbols are shorter and therefore more symbols can be transmitted over a given duration. (ii) PI- x_r is further processed to identify NCs. PCs inserted to identify the location of NCs at the Rx. It worth noting that PCs are inserted before every negative chip provided that the number of NCs is less than the number of positive chips (PoC), otherwise PCs are inserted before every positive chips. Depending on the number of inverted chips, some PCs may be padded at the end of each sequence to ensure the same length as that of the symbol duration. The last chip of the OFDM sequence is also used as the indicator to inform Rx whether the PC is inserted before the positive or negative chips. (iii) Negative inversion- Following insertion of PCs, all NCs are inverted into positive chips (PoC) with the same amplitude, which can be easily identified at Rx by checking the position of PCs. Therefore, at the Rx the chips can be checked to see if inverted, which can then be inverted back to its actual format.

2.2. The Receiver of the new system

Fig. 2 is illustrating the block diagram of PA-ACO-OFDM Rx with functionality reverse process of the Tx. Without the loos of generality, we assume the whole gain from optical source to photodiode is one. The transmitted optical signal is converted into an electrical signal $r(t)$. The shot noise modeled as an additive white Gaussian noise (AWGN) w_n is added to $r(t)$. The resulting signal $y(t) = r(t) + w_n(t)$ is passed through a low pass filter (LPF), an analog to digital converter (ADC) and the cyclic prefix (CP) removal module and yields a digital signal x_d. x_d is applied to the pilot detector module to detect the presence of the inverted signal before converting them back to the negative format using the negative regenerator process. Following the removal of PCs the output of the pilot removal processing block x_e is applied to the serial-to-parallel (S/P) converter, FFT process, de-mapping, and parallel-to-serial (P/S) converter module in order to regenerate the transmitted data.

3. SIGNAL ANALYSIS OF PA-ACO-OFDM

This section presents the details and procedure of the proposed pilot aided algorithm to achieve an improved data rate performance compared to the existing ACO-OFDM system. The analysis of the anti-asymmetric signals with PI shows that the data rates can be increased by up to almost 33% compared to the traditional ACO-OFDM. A comparison between PA-ACO-OFDM, DCO-OFDM and ACO-OFDM schemes in term of the optical power requirements is also presented. We show that the proposed system requires lower optical power (e.g., for 128-QAM) compared to DCO-OFDM. However, ACO-OFDM requires much lower optical power for all constellations.

3.1. PA-ACO-OFDM

The proposed scheme is based on ACO-OFDM, but with additional signal processing capabilities following the IFFT at the Tx including anti-symmetric removal, PC insertion and chip inversion. The serial input bit stream $b_i(t)$ is converted into parallel data streams and mapped onto the complex data symbols as given by [9], [11]:

$$S = [s_0, s_1, s_2, \dots s_{M-1}] , \quad (1)$$

where M is the number of data SCs. Let N denote the number of points in IFFT, which is equal to the total number of actual SCs. It is worth noting that, different from OFDM in RF communications, ACO-OFDM requires four times more SCs than the number of data symbols [11]. Similar to ACO-OFDM, the relationship between M and N in proposed PA-ACO-OFDM is given by:

$$M = \frac{N}{4}. \quad (2)$$

The complex symbols are mapped onto odd SCs by setting the even SCs to zero, which is given by the complex vector as:

$$Z = [0, s_0, 0 , s_1, 0, \dots , s_{M-1}], \quad (3)$$

where the size of $Z = N/2$. Z is processed by Hermitian Symmetry block (see Fig. 1) so that the output of IFFT is a real signal suitable for optical

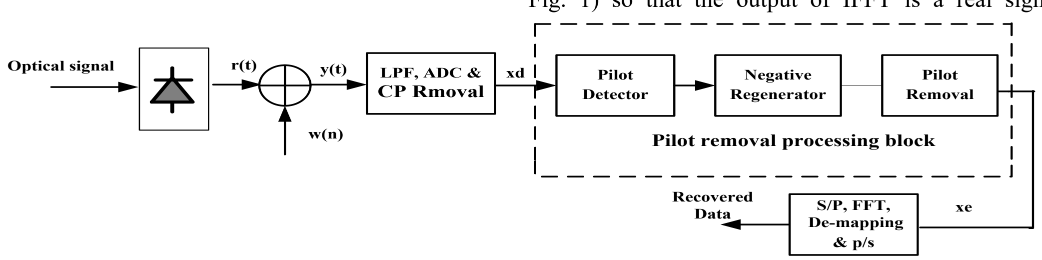

Fig. 2. Block diagram of the pilot-aided ACO-OFDM receiver

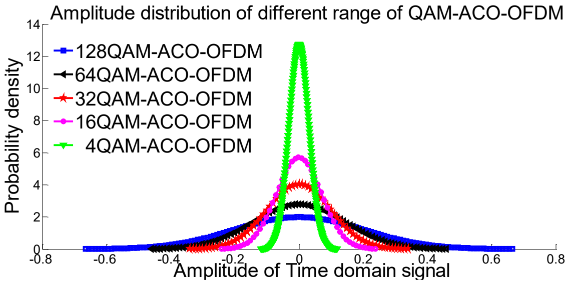

Fig. 5 Normal distribution function for different QAM data symbols of x

transmission. The Hermitian symmetry processing is defined as [9], [18]:

$$X_i = \begin{cases} Z_i & i \le N/2 - 1 \\ 0 & i = N/2 \\ Z^*_{N-i} & i \ge N/2 + 1 \end{cases},$$

$$X = [Z_0, Z_1, Z_2, Z_3, \dots, Z_{(\frac{N}{2}-2)}, Z_{(\frac{N}{2}-1)}, Z_{(\frac{N}{2})}, Z_{(\frac{N}{2}+1)}, Z_{(\frac{N}{2}+2)} \dots Z_{(N-2)}, Z_{(N-1)}],$$

$$X = \begin{bmatrix} 0, Z_1, 0, Z_3, \dots 0, Z_{(\frac{N}{2}-1)}, 0, Z_{(\frac{N}{2}-1)}^{*}, \\ 0., Z_3{}^*, 0, Z_1{}^* \end{bmatrix}. \tag{4}$$

where X_i represents the symbol to be transmitted at the i-th subcarrier (i = 0,1,..., N-1). The size of X is N, and $X \in \mathbb{C}^N$(note that $\mathbb{C}^N$ denotes the set of N-dimensional complex numbers). Since X is Hermitian symmetric, applying IFFT X yields a real anti-asymmetric time domain signal defined as [9], [12]:

$$x_k = \frac{1}{N} \sum_{i=0}^{N-1} X_i \exp\left(\frac{j2\pi ik}{N}\right), \tag{5a}$$

$$x_k = \begin{cases} x_k \text{ for } 0 \le k \le N/2 - 1 \\ -x_{k-\frac{N}{2}} \text{ for } \frac{N}{2} \le k < N - 1 \end{cases}, \tag{5b}$$

where x_k, referred to as a chip with a constant duration of T_s, is the k^{th} time domain sample of x, $k = 0,1,..,N-1$. $x \in \mathbb{R}^N$and, $\mathbb{R}^N$ denotes a set of N-dimensional real numbers. Since ACO-OFDM symbols contain N-chip the number of time slot required for each ACO-OFDM symbol is given by:

$$N_{T_s-ACO_T} = N. \tag{6}$$

Error! Reference source not found.**Error! Reference source not found.** illustrates the anti-asymmetric time domain signal for the existing ACO-OFDM as described in (5b). For example, the chip 0 is anti-symmetric with chip 16, chip 2 is anti-symmetric with chip 17 and so on. From the viewpoint of information redundancy, these chips convey the same but inverted information, i.e., redundancy, which is the waste of bandwidth (equivalently, part of the time duration of OFDM symbol is also wasted). It can be understood as half of the ACO-OFDM chips are used to transmit the information data and the other half are the overhead chips for maintaining the anti-symmetric properties.

Different to the traditional ACO-OFDM, the proposed scheme includes additional modules of the anti-symmetric signal removal, PC insertion, chip inversion as shown in

Fig. 1, which are introduced to reduce the number of time slots for transmitting the same amount of data. It is shown that the redundant chips in the 2nd half of the OFDM symbol can be removed without losing the information content at the cost of inserting additional PCs to the chip sequence. However, the advantage is that the number of PCs in PA-ACO-OFDM is half the number of the redundant chips in ACO-OFDM. In the proposed scheme the IFFT output passed through the anti-symmetric removal module, (see Fig. 4), and the output of the anti-symmetric removal module is given as:

$$\boldsymbol{x_r} = [\boldsymbol{x_0}, \boldsymbol{x_1}, \boldsymbol{x_2}, \dots \dots, \boldsymbol{x_{(\frac{N}{2}-1)}}]. \tag{7}$$

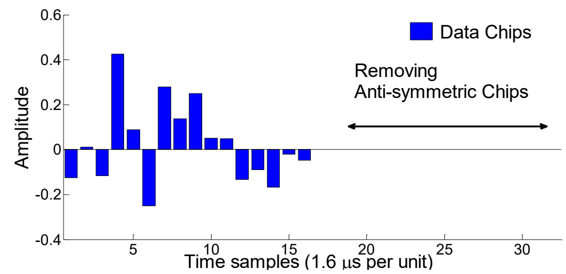

Fig. 4 Signals in the time domain for ACO-OFDM after anti-asymmetric removal process

Once all redundant chips in the 2nd half of the IFFT output sequence are removed, PCs with higher amplitude are inserted into the sequence x_r at some location. Then the negative chips are inverted to positive in the negative inversion process module. This is to meet the non-negative signal transmission requirement in optical communications, (see Fig. 3).

The PCs will be used by the Rx to identify if the received chips were inverted at the Tx. However, in order to reduce the number of inserted PCs, we first need to determine the number of NCs, if the number of NCs is less than half of the total number of chips (i.e., there are less NCs than PoC), then PCs are inserted before every negative chip. If the number of NCs is greater than the number of PoC, then PCs are inserted before every positive chip. As a result, the number of PCs will be maintained to less than or equal to N/4. Since the number of PoC and NC are different for different OFDM symbols, in order to keep the length of every OFDM symbol fixed, a number of PCs are padded at the end of chip sequences. Furthermore, a special PC is inserted at the end of the sequence to indicate the locations of PCs. Note that, in ACO-OFDM the number of time slot is N, therefore the duration of an ACO-OFDM symbol is $N{\cdot}T_s$. However, for the proposed scheme, the

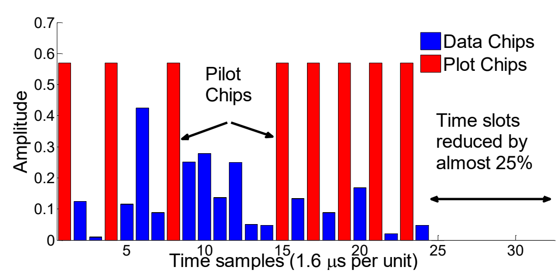

Fig. 3 Pilot chips insertion

length of the OFDM symbol is fixed and equal to 3/4· ($N{\cdot}T_s$).

3.2. Selecting the Pilot's Amplitude

The normal distributions with mean µ and standard deviation σ of the probability density x for a range of QAM–ACO-OFDM schemes are shown in Fig. 5. Based on the confidence interval A_d of 99.74%, the amplitude of data chips is below A_d which is given as:

$$A_d = \mu + 3\,\sigma. \tag{8}$$

At the Rx, in order to be able to detect the PC from the rest of the data chips and remove it prior to FFT we have assigned higher amplitudes to PCs, which are higher than A_d (i.e., 99.74 % of the amplitude of data chips). Considering the AWGN noise the amplitude of PC is as:

$$\boldsymbol{A_p = \alpha A_d} \,, \tag{9}$$

where the coefficients $\alpha > 1$. Of course noise will affect amplitudes of data chips and PCs. At Rx to detect the PC from the rest of the data chips and remove it prior to FFT, we have adopted the threshold detection scheme with the threshold level defined as:

$$A_t = \beta A_d \,, \tag{10}$$

where ($\alpha > \beta > 1$). Both coefficients (α and β) are related to the noise power as will be shown later in section 4. Note that at Rx all the chips above A_t are considered as PC.

The confidence intervals for 4-, 16-, 32-, 64-, and 128-QAM are illustrated in Table I. Note that since the PAPR is proportional to the number of SCs [19], we have only shown A_d for $N = 1024$.

3.3. PA-ACO-OFDM data rates

Due to the anti-symmetric chips removal, the number of data chips in the proposed scheme is half of the data chips in the traditional ACO-OFDM (see **Error! Reference source not found.**. Therefore the total number of time slots required to transmit M-data symbols in the proposed scheme is given by:

$$\boldsymbol{N_{Ts-PA} = \frac{1}{2}N + N_{PC\,1} + N_{PC2} + N_{PC3}} \,, \tag{11}$$

where N_{PC1} the number of PCs is inserted prior to the inversion process and N_{PC2} is the number of padding PCs to ensure that the frame length is fixed to $\frac{3}{4} \cdot (N.Ts)$. N_{PC3} , represent the number of chips inserted at the end of the sequence. Without loss of generality, we can use only one PC for N_{PC3} , that is $N_{PC3} = 1$.

Table I

THE CONFIDENCE INTERVAL VALUES FOR A RANGE QAM

QAM order	4	16	32	64	128
Confidence interval A_d	0.0935	0.2096	0.29	0.43	0.6

The data rate for the traditional ACO-OFDM with no cyclic prefix is defined in [19]:

$$\boldsymbol{R^{\{ACO\}} = \frac{M-1}{N_{Ts-ACO}} \; B \log_2 L}, \tag{12}$$

where B is the bandwidth and L is the modulation order.

The data rate of the proposed PA-ACO-OFDM can be defined as:

$$R^{\{PA\}} = \frac{M-1}{N_{TS-PA}} \; B \log_2 L \,, \tag{13}$$

Thus

$$\boldsymbol{R^{\{PA\}} \simeq 1.33 \; R^{\{ACO\}}} \tag{14}$$

From equation (14) it can be clearly seen that R offered by the proposed scheme is higher by almost 33 % compared to the traditional ACO-OFDM. The achievable R for ACO-OFDM, PA-ACO-OFDM and DCO-OFDM for 4-, 16-, 32-, 64- and 128-QAM are showed in Table II. Note that, both even and odd subcarriers are modulated in DCO-OFDM (see section 1).

3.4. Power consumption

In PA-ACO-OFDM the penalty paid for the increased in R is the optical power compared to the ACO-OFDM. In LED based VLCs the average transmit optical power P_T for ACO-OFDM, DCO-OFDM [11] and PA-ACO-OFDM are given as:

$$P_{T-ACO} = \frac{1}{\sqrt{2\pi} F_T} \sum_{d=1}^{F_T} \sigma_{ACO}, \tag{15}$$

Table II

DATA RATES FOR ACO-OFDM, PA-ACO-OFDM AND DCO-OFDM FOR A RANGE OF QAM

	Data rate R (M bit/s)				
QAM	4	16	32	64	128
DCO-OFDM	19.92	39.48	49.8	59.76	69.72
PA-ACO-OFDM	13.26	26.52	33.16	39.79	46.42
ACO-OFDM	9.96	19.92	24.9	29.88	34.86

$$P_{T-PA-ACO} = \frac{1}{\sqrt{2\pi} F_T} \sum_{d=1}^{F_T} \sigma_{PA-ACO}, \tag{16}$$

$$P_{T-DC} = \frac{\sigma_D}{2\pi} \exp\left(\frac{-B_{DC}^2}{2\sigma_D^2}\right) + B_{DC}\left(1 - Q\left(\frac{B_{DC}}{\sigma_D}\right)\right), \tag{17}$$

where F_T is total number of transmitted OFDM symbols within the test period (i.e., d = 1, 2,... F_T and F_T = 10000), σ_{ACO} and σ_D are the standard deviations of the time domain signal for ACO-OFDM, and DCO-OFDM [11], and σ_{PA-ACO} is the slandered deviation of the time domain signal for PA-ACO-OFDM given as; $\sigma_{PA-ACO} = E\{x_{PA-ACO}^2\}$ (see Fig. 1). In (17) $B_{DC} = \eta\sqrt{E\{x(t)^2\}}$ is the required DC bias level to ensure non-negative OFDM signal, where η is the proportionality constant.

Table III illustrates P_T for transmitting a frame of ACO-OFDM, DCO-OFDM and PA-ACO-OFDM for 4-, 16-, 32-, 64-and 128 QAM, α= 2.7 (see section 4), and $\eta = 2$ as in [9]. From Table III it can clearly be seen that ACO-OFDM requires less P_T compared to DCO-OFDM and PA-ACO-OFDM for constellations up to 128-QAM. Also it can be observed that the required P_T for PA-ACO-OFDM is less than one for DCO-OFDM, so that for 4-QAM, DCO-OFDM requires P_T almost 10 times more than PA-ACO-OFDM.

As an example, Fig. 7 show simulated 1024 time-domain chip sequences for DCO-OFDM, ACO-OFDM and PA-ACO-OFDM for 4-QAM (without cyclic prefix). Note that for PA-ACO-OFDM α =2.7 (see section 4).

From Fig. 7 it can be observed that ACO-OFDM requires less power than DCO-OFDM and PA-ACO-OFDM. It's also shows that the time duration of PA-ACO-OFDM symbol is less than the time duration of DCO-OFDM and ACO-OFDM symbols for the same number of subcarriers.

4. SIMULATION RESULTS

Table III

NORMALIZED TRANSMIT OPTICAL POWER PT FOR A RANGE OF QAM

	Normalized transmitted optical power				
QAM	4	16	32	64	128
DCO-OFDM	0.0957	0.2139	0.3027	0.4384	0.6126
PA-ACO-OFDM	0.0083	0.0415	0.0829	0.1742	0.34
ACO-OFDM	0.000385	0.0019	0.0039	0.0082	0.016

Simulation results are presented in this section. We have considered 1024-IFFT points and because of the IM/DD requirements, 512 and 256 SCs were used for the data signal in DCO-OFDM and in both ACO-OFDM and PA-ACO-OFDM, respectively. Table IV lists all the key parameters adopted in the simulation of the proposed scheme. The cyclic prefix duration is chosen to be equal to the maximum delay of a typical VLC multipath channel as in [19]. As discussed earlier, the OFDM symbol duration is reduced in PA-ACO-OFDM because of reduced number of chips, therefore R is improved

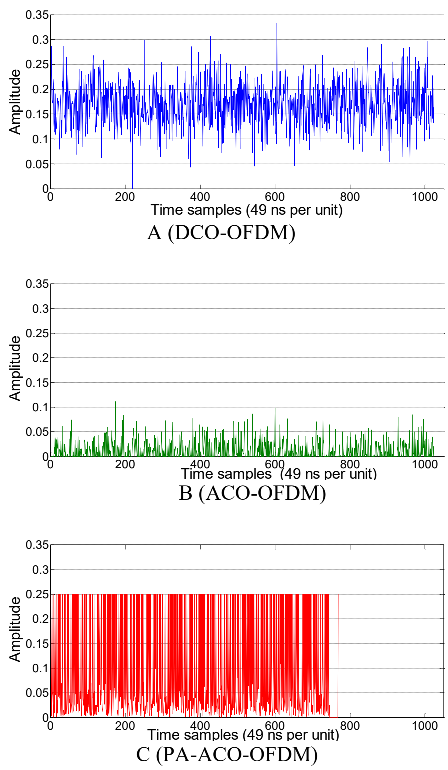

Fig. 7. Time domain waveforms for DCO-OFDM, ACO-OFDM and PA-ACO-OFDM

compared to ACO-OFDM, Additionally, the power efficiency and the BER performance of the new system improved by adjusting the amplitude of the PCs.

To determine the best values for α and β we have simulated the BER performance of the proposed scheme for a range of SNR as shown in Fig. 6 As can be seen from Fig. **6**, the BER performance improves with increasing values of α and β reaching noise floor levels where there is no further improvement for $\alpha >> \alpha_{op}$ and $\beta >> \beta_{op}$. The best and worth BER

Table IV

SIMULATION PARAMETERS

Parameter	Value
LED type	Blue
LED bandwidth	20 MHz
IFFT length	1024
Number of frames	10000
Modulation type and order	4, 16, 32, 64, 256, 1024 QAM
Coding rate	None
Subcarrier spacing	≈ 19.53 kHz
DCO-OFDM symbol duration	51.2 µs
ACO-OFDM symbol duration	51.25 µs
PA- ACO-OFDM symbol duration	≈38.45 µs
Cyclic prefix duration	50 ns

performance is achieved for the SNR of 16 dB and 4 dB, respectively. The optimum values of α and β are within the ranges of $2.5 < \alpha_{op} < 2.6$ and $1.75 < \beta_{op} < 1.95$, where the BER noise floors are observed.

Next we set $\beta = 1.85$ and investigate the BER performance against the SNR for α_{op} of 2.7, 2.45 and 2.35 obtained from Fig. 6 as shown in Fig. 8 Also depicted for comparison is the BER performance for the standard 4-QAM ACO-OFDM with no PC. As can be seen the proposed ACO-OFDM with α_{op} of 2.7 displays a similar performance to ACO-OFDM with no PCs. For $\alpha_{op} = 2.45$ the BER performance is the same as ACO-OFDM with no PCs for SNR ≥ 8 dB. For $\alpha_{op} = 2.35$ the BER performance of the ACO-OFDM with PC is inferior to the ACO-OFDM with not PCs for SNR < 12 dB. This is because of the increased probability of the false alarm associated with the detection of PC. The same values of α_{op} were also used in higher order QAM

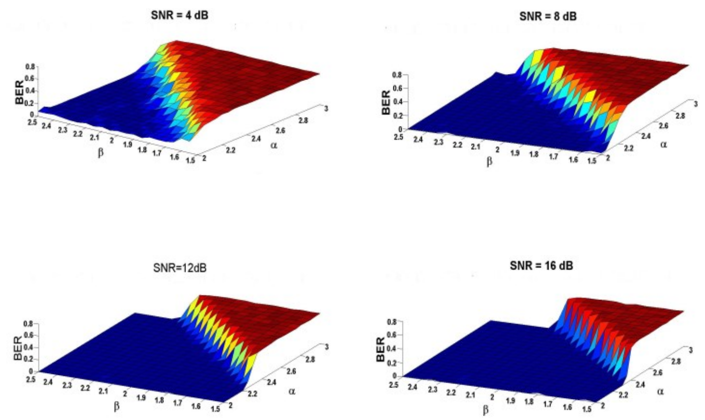

Fig. 6 BER against $\boldsymbol{\alpha}$ and β for a range of SNR for 4QAM-PA-ACO-OFDM

including 1024-IFFT points ACO-OFDM for $\beta = 1.85$ and the BER results obtained confirmed that α_{op} of 2.7 should be adopted for all values of SNR.

Finally, Fig. 9 illustrates the simulation results for the data throughput as a function of the SNR for 4-QAM DCO-OFDM, ACO-OFDM and PA-ACO-OFDM. To determine the link throughput, the received corrected bits are divided by the length of each OFDM symbol for range of SNR. For both ACO-OFDM and PA-ACO-OFDM the throughput reaches the saturation levels at a SNR of ~6 dB. This is PC were not taken into account in the SNR analysis. Note that the system throughput for DCO-OFDM reaches the saturation level at a SNR of ~15 dB because of the DC bias requirement. For both DCO-OFDM and the PA-ACO-OFDM the throughputs are higher by about 50% and 32% compared to the ACO-OFDM. This is due to both even

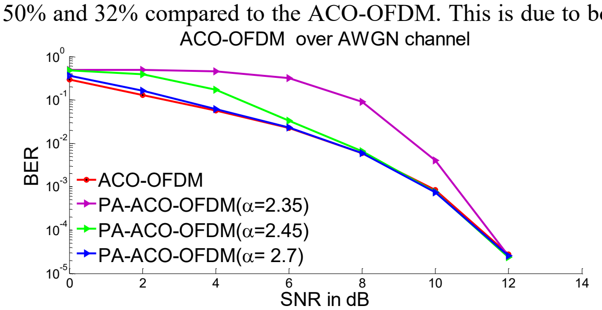

Fig. 8. BER vs. SNR for 4-QAM ACO-OFDM and PA-ACO-OFDM with different values of $\boldsymbol{\alpha}$

and odd SCs used to transmit the data in DCO-OFDM. In the proposed scheme, almost 25% of time slots per OFDM symbol are reduced.

5. CONCLUSION

In this paper a novel PA- ACO-OFDM was proposed and simulated, where the advantages of anti-asymmetric time domain characteristics of ACO-OFDM was exploited in order to increase the data rate by decreasing the symbol duration. Results presented showed that the data rate of the proposed PA-ACO-OFDM is increased by almost 33% compared to the conventional ACO-OFDM. We also showed that the power efficiency and the BER performance of the PA-ACO-OFDM can be improved by varying the amplitude of the pilot chips. Furthermore, comparison between PA-ACO-OFDM and DCO-OFDM in term of optical power was presented and it has

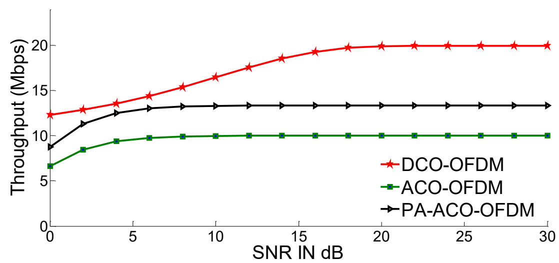

Fig. 9. Throughput against the SNR for 4-QAM DCO-OFDM, ACO-OFDM and PA-ACO-OFDM

showed that the new system required less optical power. In addition, the inserted high amplitude PCs can be effectively utilized for illumination, and dimming control as well as channel estimation, equalization and modulation rate adjustment in VLCs, which is the subject of future research work.

References

[1] Z. Ghassemlooy, W. Popoola, and S. Rajbhandari*, Optical wireless communications: system and channel modelling with Matlab.* London,UK.: CRC Press, 2012.

[2] T. Komine and M. Nakagawa, "Fundamental analysis for visible-light communication system using LED lights,“ *IEEE Transactions on, Consumer Electronics*, vol. 50,no. 1, pp. 100-107, Feb, 2004.

[3] Z. Hua, Y. Ying, and X. Wei, "PAPR reduction for DCO-OFDM visible light communications via semidefinite relaxation,“ *IEEE, Photonics Technology Letters*, vol. 26, no. 17, pp. 1718–1721, Sep, 2014.

[4] W. Qi, W. Zhaocheng, and D. Linglong, "Asymmetrical hybrid optical OFDM for visible light communications with cimming control,“ *IEEE, Photonics Technology Letters*., vol. 27,no. 9, pp. 974-977, May. 2015.

[5] Y. S. Cho, J. Kim, W. Y. Yang, and C. G. Kang, MIMO-OFDM Wireless Communications with MATLAB, Singapore.: IEEE Press, 2010.

[6] W. O. Popoola, Z. Ghassemlooy, and B. G. Stewart, "Pilot-assisted PAPR reduction technique for optical OFDM communication systems,“ *Journal of Light wave Technology*. , vol. 32, no. 7, pp. 1374–1382, Apr, 2014.

[7] Z. Yu, R. J. Baxley, and G. T. Zhou, "Peak-to-average power ratio and illumination-to-communication efficiency considerations in visible light OFDM systems.,“ *IEEE International Conference on, Acoustics, Speech and Signal Processing (ICASSP).,* May 2013, vol. 22, pp. 5397-5401.

[8] M. Z. Afgani, H. Haas, H. Elgala, and D. Knipp, "Visible light communication using OFDM,“ In *2nd International Conference on Testbeds and Research Infrastructures for the Development of Networks and Communities* 2006, p. 134, 6 pp.

[9] J. Armstrong, B. Schmidt, D. Kalra, H. A. Suraweera, and A. J. Lowery, "Performance of asymmetrically clipped optical OFDM in AWGN for an intensity modulated direct detection system,“ In *IEEE, Global Telecommunications Conference, GLOBECOM*, 2006.pp. 1-5.

[10] S. D. Mohamed, H. S. Khallaf, H. Shalaby, I. Andonovic, and M. H. Aly, "Two approaches for the modified asymmetrically clipped optical orthogonal frequency division multiplexing system,“ in *Japan-Egypt International Conference Electronics, Communications and Computers (JEC-ECC)*, 2013 , pp. 135-139.

[11] S. D. Dissanayake and J. Armstrong, "Comparison of ACO-OFDM, DCO-OFDM and ADO-OFDM in IM/DD systems,“ *Journal of Light wave Technology*, vol. 31, no. 7, pp. 1063–1072, Apr. 2013.

[12] S. C. J. Lee, S. Randel, F. Breyer, and A. J. Koonen, "PAM-DMT for intensity-modulated and direct-detection optical communication systems,“ *IEEE Photonics Technology Letters.,* vol. 21, no. 23, pp. 1749–1751, Dec. 2009.

[13] D. Tsonev, S. Sinanovic, and H. Haas, "Novel unipolar orthogonal frequency division multiplexing (U-OFDM) for optical wireless,“ In *IEEE Vehicular Technology Conference (VTC Spring)*, May 2012, pp. 1-5.

[14] S. D. Dissanayake, K. Panta, and J. Armstrong, "A novel technique to simultaneously transmit ACO-OFDM and DCO-OFDM in IM/DD systems,“ In *IEEE, GLOBECOM Workshops (GC Wkshps),* 2011, pp. 782-786.

[15] J. Armstrong and B. Schmidt, "Comparison of asymmetrically clipped optical OFDM and DC-biased optical OFDM in AWGN,“ *IEEE Communications Letters*, vol. 12, no. 5, pp. 343-345, May 2008.

[16] I. Stefan, H. Elgala, and H. Haas, "Study of dimming and LED nonlinearity for ACO-OFDM based VLC systems,“ In *IEEE Wireless Communications and Networking Conference (WCNC),* 2012, pp. 990-994.

[17] Z. Yu, R. J. Baxley, and G. T. Zhou, "EVM and achievable data rate analysis of clipped OFDM signals in visible light communication,“ *EURASIP Journal on Wireless Communications and Networking,* vol. no. 321, pp. 1-16,Oct 2012.

[18] R. Mesleh, H. Elgala, and H. Haas, "On the performance of different OFDM based optical wireless communication systems,“ *Journal of Optical Communications and Networking, IEEE/OSA,* vol. 3, no. 8, pp. 620–628, Aug. 2011.

[19] H. Elgala, R. Mesleh, and H. Haas, "Practical considerations for indoor wireless optical system implementation using OFDM.“ Conference in Telecommunications, Zagreb, Croatia, 2009, pp. 25–30.